

# On the Azimuthal Stability of Shock Waves around Black Holes

Diego Molteni

Dipartimento di Scienze Fisiche ed Astronomiche Università di Palermo Via Archirafi 36,  
90123 Palermo, Italy

Gábor Tóth

Department of Atomic Physics, Eötvös University, Pázmány sétány 2, Budapest 1117,  
Hungary

and

Oleg A. Kuznetsov

Keldysh Institute of Applied Mathematics Miusskaya sq. 4, 125047 Moscow, Russia

## ABSTRACT

Analytical studies and numerical simulations of time dependent axially symmetric flows onto black holes have shown that it is possible to produce stationary shock waves with a stable position both for ideal inviscid and for moderately viscous accretion disks.

We perform several two dimensional numerical simulations of accretion flows in the equatorial plane to study shock stability against *non-axisymmetric azimuthal perturbations*. We find a peculiar new result. A very small perturbation seems to produce an instability as it crosses the shock, but after some small oscillations, the shock wave suddenly transforms into an asymmetric closed pattern, and it stabilizes with a finite radial extent, despite the inflow and outflow boundary conditions are perfectly symmetric.

The main characteristics of the final flow are: 1) The deformed shock rotates steadily without any damping. It is a permanent feature and the thermal energy content and the emitted energy vary periodically with time. 2) This behavior is also stable against further perturbations. 3) The average shock is still very strong and well defined, and its average radial distance is somewhat larger than that of the original axially symmetric circular shock. 4) Shocks obtained with larger angular momentum exhibit more frequencies and beating phenomena. 5) The oscillations occur in a wide range of parameters, so this new effect may have relevant observational consequences, like (quasi) periodic oscillations, for the accretion of matter onto black holes. Typical time scales for the periods are 0.01 and 1000 seconds for black holes with 10 and  $10^6$  solar mass, respectively.

*Subject headings:* accretion, accretion disks — instability — shock waves

## 1. Introduction

Shock waves in rotating accretion flows onto compact objects present a very important mechanism to transform the potential gravitational energy into radiation. The possibility that they exist also around black holes (BH) has been suggested years ago by Hawley, Smarr, & Wilson (1984a, 1984b). However their shocks were unstable in radial direction. Recently it has been shown that there is a wide range of parameters (namely specific angular momentum and initial temperature) for which steady shock configurations are possible (Chakrabarti 1989, 1990; for viscous flows see Chakrabarti & Molteni 1993, Lanzafame et al. 1998). Essentially the shock position depends on thermal energy and angular momentum contents of the flow: the balance between the centrifugal and total pressure forces (ram plus internal) is the main factor determining the shock formation. The stability was examined with axially symmetric numerical calculations (Molteni, Lanzafame, & Chakrabarti 1994; Chakrabarti & Molteni 1995). Recent analytical studies (Lu & Yuang 1997; Nakayama 1993, 1994) have also shown the stability of isothermal and adiabatic shocks against axially symmetric perturbations.

The stability of shock waves in accretion flows has great astrophysical relevance since, in this way, the emission due to the shock is not a transient episode, but can be a permanent mechanism responsible of the radiated energy. However, the studies made up to now are all in axial symmetry.

In this paper we examine the azimuthal stability of the initially axisymmetric shocks by perturbing them with an *asymmetric perturbation*. We explore the parameter space defined by the angular momentum and temperature of the accreted gas. The computations are done in the equatorial plane assuming slab symmetry in the  $z$  direction (thin disk approximation). We use two different computer codes to integrate numerically the hydrodynamic equations: the Versatile Advection Code (VAC, Tóth 1996, 1997, also see <http://www.phys.uu.nl/~toth/>) and another one developed by Kuznetsov (Kuznetsov et. al. 1998).

Here we are not discussing the origin of the supersonic accretion flow and the influence of viscosity. The formation of supersonic flows in the accretion disk has been predicted by various authors in different contexts valid both for galactic and extragalactic supermassive Black Holes (for viscous transonic flows cfr. Chakrabarti 1996, for advection dominated flows see Gammie and Popham 1998, Igumenshev, Abramowicz, & Novikov 1998, Narayan, Mahadevan, & Quataert 1998). These works clearly show that since the viscous time scale is much longer than the infall time scale close to the black hole, the angular momentum remains almost constant, unless the viscosity is really very high (i.e. the  $\alpha$  parameter close to unity). The supersonic region is well inside the accretion disk (typically within 50

Schwarzschild radii), far from the impact of any accretion stream that typically occurs at  $10^6$  Schwarzschild radii. Therefore the supersonic inflow is expected to be approximately axisymmetric. Small non-axisymmetric perturbations may occur, of course, which is exactly the motivation for our study.

The paper is structured as follows. Sections 2 and 3 describe the analytic and numerical models, respectively, the results of the numerical simulations are presented in Section 4, and conclusions with our plans for further investigations are discussed in Section 5.

## 2. Modeling the problem

We solve numerically the hydrodynamic equations describing the time dependent motion of a rotating, inviscid, ideal gas falling into a Schwarzschild black hole. We assume an initial axisymmetric configuration and a permanent axisymmetric boundary condition inflow. Since our study concerns the inner regions of the accretion disk ( $r \leq 50r_g$ ) we may disregard the possible perturbation due to spiral shocks (Yukawa et al. 1997). Indeed, the validity of the extension of their result interior into the disk is far to be clear. Furthermore, the phenomenon, we discuss, may occur in accretion onto black holes in galactic nuclei, where a fully axisymmetric boundary condition may easily occur. To allow for analytical comparison and to be able to study the phenomenon with reasonable computer time, the motion is restricted to the  $z = 0$  plane and we assume that gradients in the  $z$  direction are negligible, i.e.  $\partial/\partial z = 0$ . The general relativistic effects are taken into account by using the Paczyński & Wiita (1980) pseudo-Newtonian gravitational potential

$$\Phi(r) = -\frac{GM}{r - r_g} = -\frac{c^2}{2(r/r_g - 1)}, \quad (1)$$

where  $r, G, c, M$  and  $r_g$  are the radial distance, the gravitational constant, the speed of light, and the mass and the Schwarzschild radius ( $r_g = 2GM/c^2$ ) of the accreting object, respectively. This approximation is frequently used when accurate relativistic details are not required. The results show that both the initial axisymmetric and the final distorted shocks form at radial distances ( $r \geq 5r_g$ ) for which the pseudo-Newtonian potential is fairly accurate.

We solve the equations of hydrodynamics in polar coordinates  $r$  and  $\varphi$  for mass density  $\rho$ , radial momentum density  $\rho v_r$ , angular momentum density  $r\rho v_\varphi$  and energy (kinetic+thermal) density  $e$ . The four equations express conservation of mass, radial momentum balance, conservation of angular momentum, and energy balance, respectively.

$$\frac{\partial r\rho}{\partial t} + \frac{\partial r\rho v_r}{\partial r} + \frac{\partial r\rho v_\varphi}{\partial \varphi} = 0 \quad (2)$$

$$\frac{\partial r \rho v_r}{\partial t} + \frac{\partial}{\partial r}(r \rho v_r^2 + r p) + \frac{\partial}{\partial \varphi}(\rho v_r v_\varphi) = \rho v_\varphi^2 + p - r \rho \frac{\partial \Phi}{\partial r} \quad (3)$$

$$\frac{\partial r^2 \rho v_\varphi}{\partial t} + \frac{\partial}{\partial r}(r^2 \rho v_r v_\varphi) + \frac{\partial}{\partial \varphi}(r \rho v_\varphi^2 + r p) = 0 \quad (4)$$

$$\frac{\partial r e}{\partial t} + \frac{\partial}{\partial r}[r v_r (e + p)] + \frac{\partial}{\partial \varphi}[v_\varphi (e + p)] = -r \rho v_r \frac{\partial \Phi}{\partial r} \quad (5)$$

where the thermal pressure is  $p = (\gamma - 1)[e - \rho(v_r^2 + v_\varphi^2)/2]$  with the polytropic index  $\gamma = 4/3$ , which is appropriate for relativistic gas. We adimensionalize our equations by using the Schwarzschild radius and the speed of light as reference units, i.e.  $r_g = 1$  and  $c = 1$ .

The outer boundary of the computational domain is set far away from the BH at a radius  $r_{max}$  (typically  $r_{max} \sim 20 - 50 r_g$ ), but closer than the outer sonic point, so that the inflow is supersonic. The inner boundary is chosen at a distance  $r_{min}$  inside the inner sonic point where the flow behind the shock becomes supersonic again due to the gravitational acceleration. Typically we take  $r_{min} \sim 1.5 r_g$ . The boundary conditions are periodic for the  $0 \leq \varphi < 2\pi$  coordinate.

Since the equations are linear in the mass and energy densities, we may choose the density of the infalling gas at the outer boundary of the computational domain to be unity,  $\rho(r_{max}) = 1$ . Once the density scale is fixed, the steady state solution is fully determined by three conserved quantities: the accretion rate  $A = r \rho v_r$ , the specific angular momentum  $\lambda = r v_\varphi$  and the Bernoulli constant  $B = \Phi + (e + p)/\rho$  (sometimes referred to as ‘energy’). To match the full solution, which contains an outer sonic point outside the domain, the accretion rate cannot be chosen independently of the other two constants, rather it should be calculated from the set of the algebraic equations expressing the mass conservation, the energy conservation and the polytropic equation of state following the procedure outlined in the Appendix. The remaining two parameters, the angular momentum and the Bernoulli constant can be chosen such that the steady shock is positioned at a distance  $r_{shock}$ . The dependence of the shock position on  $\lambda$  and  $B$  is shown in Fig. 1 in the parameter range of our test cases. The supersonic inflow parameters are independent of the azimuthal coordinate  $\varphi$  and, if not perturbed, the initial steady state flow would remain axi-symmetric forever.

The initial condition is the steady solution perturbed a few units upstream of the shock at  $r_{perturb} \sim r_{shock} + 3 r_g$  and  $\varphi = \pi$  in a small region of size  $\Delta r = r_{perturb} \Delta \varphi = 0.05 r_{perturb}$ . We typically perturb the pressure or the density by a few per cent only, therefore the energy and momentum content of the perturbation is completely negligible relative to the respective quantities for the full domain. The perturbation is advected into the BH with

the flow as shown by the upper panels of Fig. 2.

### 3. Numerical scheme

To integrate numerically the hydrodynamic equations (2)-(5), we use two different programs, VAC (Tóth 1996, 1997) and another code implemented by Kuznetsov (Kuznetsov et. al. 1998). Both codes use Total Variation Diminishing (TVD, Harten 1983) type schemes. In VAC we used a characteristic based Lax-Wendroff type TVD scheme with a Roe type approximate Riemann solver (Roe 1986) and minmod or Woodward flux limiters (see Tóth & Odstrčil 1996 for details), while in the other code a Lax-Friedrichs type scheme is applied with Osher-Chakravarty anti-diffusion term (Chakravarty & Osher 1985). The combined Lax-Friedrichs-Osher scheme was suggested by Vyaznikov, Tishkin, & Favorsky(1989). Here the  $r$  and  $\varphi$  fluxes are added at the same time, while VAC uses a Strang type dimensional splitting. Both schemes are 2nd order accurate in space, the VAC code is temporally second order too, while the other code is only first order accurate in time. There are further differences in the grid settings and in the implementation of many numerical details. We have checked for several cases that the two codes give essentially identical results.

The analytical equations are discretized in conservation form. In both codes, the physical and numerical fluxes are calculated for the angular momentum density  $r\rho v_\varphi$  instead of the usual tangential momentum density  $\rho v_\varphi$  to achieve better angular momentum conservation. In VAC, this does not require the modification of the approximate Riemann solver itself, only the obtained fluxes are handled differently.

Another concern is the temporally accurate evaluation of source terms on the right hand sides of the equations (3) and (5), which arise from the curvature of the coordinate system and the gravitational force of the BH. The Lax-Friedrichs-Osher code is only first order accurate in time, thus very small time steps are used (Courant number  $\approx 0.1$ ). In VAC, we follow the algorithm described by Ryu et. al. (1995) in their Appendix with a correction of their equation (A22), which should read  $\bar{q}^{n+1/2} = (q^n + q_{hydro}^n + S^n)/2$ , to achieve second order accuracy. This allows larger time steps with Courant numbers  $\approx 0.8$ . A naive implementation of a Lax-Wendroff type TVD scheme in polar coordinates leads to first order temporal accuracy and very inaccurate steady state shock positions for Courant numbers close to unity.

Boundary conditions are easily implemented with two layers of ghost cells surrounding the physical domain. Supersonic inflow and outflow can be realized with *fixed* and

*extrapolated* ghost cell values, respectively. The fixed cell values are derived from the flow parameters: the accretion rate  $A$ , angular momentum  $\lambda$ , and the Bernoulli constant  $B$ , which are listed for all the test cases in Table 1. Periodicity in the  $\varphi$  direction is trivial to maintain.

Convergence of the numerical results was checked by redoing the same calculation with different grid resolutions  $N_r \times N_\varphi = 200 \times 60, 200 \times 120, 200 \times 100$ , and  $300 \times 90$ . We also have the option of using a logarithmic grid spacing in the  $r$  direction (typically we use  $\Delta r_{j+1}/\Delta r_j \approx 1.003$ ), which allows a better resolution of sharp gradients close to the BH. The results were found to be extremely similar on all grids. The evolution becomes qualitatively wrong only for a very coarse grid spacing  $100 \times 30$ , where the oscillations are suppressed by numerical diffusion and the perturbed shock returns to the symmetric steady state after a short transient. We may conclude that the results are not too sensitive to a small amount of dissipation.

Although an analytical steady state can be easily derived by solving ordinary differential equations (Chakrabarti & Molteni 1993), it is better to obtain a *numerical equilibrium*, which is always slightly different from the analytical steady state solution due to the discretization errors. In particular, VAC can solve the time dependent axially symmetric one dimensional equations starting from a crude initial condition. The most efficient way to converge to steady state is to do a 1D simulation with axial symmetry employing a fully implicit time stepping algorithm (see Tóth, Keppens, & Botchev 1998 for details).

The 1D equilibrium solution is ‘rotated’ around the symmetry axis to get the starting configuration for the 2D runs, i.e. the 2D variables  $w^{(2D)}(i_r, i_\varphi) = w^{(1D)}(i_r)$  for  $w = \rho, \rho v_r, r \rho v_\varphi, e$ , where  $i_r, i_\varphi$  are the grid indices. The radial grid spacing must be the same for the 2D and 1D grids, but the number of grid points in the  $\varphi$  direction can be chosen freely. We have tested that *without* the non-axisymmetric perturbation the 2D steady state obtained this way is stable and no fluctuations are introduced in the flow, since the numerical scheme used for the 2D simulation is the same as for the 1D simulation.

Once a steady solution with the shock is obtained, the small perturbation described at the end of the previous section is added in the cells around  $r = r_{\text{perturb}}$ ,  $\varphi = \pi$  and the flow is evolved with the 2D code using explicit time stepping for hundred thousands of time steps.

## 4. Results

Several test cases were studied in the parameter space defined by the specific angular momentum  $\lambda = rv_\varphi$  and the Bernoulli constant  $B = \Phi + (e + p)/\rho$ . Beside  $\lambda$  and  $B$ , Table 1 also lists the scaled accretion rate  $A/\rho(r_{max}) = -rv_r\rho/\rho(r_{max})$ , which is necessary for setting up the boundary conditions, and the shock position  $r_{shock}$  for the axially symmetric steady state, which can be obtained by the procedure described in the Appendix. The cases are ordered by the radial shock distance and the specific angular momentum: the bigger case numbers (1, 2, ... 5) correspond to larger  $r_{shock}$ , and the subcases (a, b, ...) have larger and larger  $\lambda$ , respectively. The outer boundary is located at  $r_{max} = 56, 20, 25, 50$  and  $56$  for the five cases respectively.

To check for time variations, we monitor the flow for the maximum shock radial distance, for the shock position at  $\varphi = 0$ , and for the mass and thermal energy contents of different sectors and annuli. We also analyzed snapshots at different times (see Fig. 2), and visualized the simulation with animations.

All cases, except the stable case 4, evolve rather similarly. As the perturbation crosses the hot subsonic postshock region, the shock becomes slightly distorted, and it oscillates with a small amplitude. After this transient, the phases of the small oscillations synchronize, and a very clear distorted shock develops with the end closed back as shown by Fig. 3. Further details of the final shock structure can be studied on Fig. 3.

The new axially asymmetric shock, with a dominant  $m = 1$  mode, reaches a new “quasi steady state” with finite radial extent (in case 5b the simulation had to be stopped when the shock touched the outer boundary of the computational domain). The radial distance range of the twisted shock is not very different from the axially symmetric shock position  $r_{shock}$ . The quasi steady state means that the flow changes periodically, without any sign of damping or instability. In case of “regular oscillations” the flow pattern rotates like a solid body with a period  $P$ , so it is a true steady state in the co-rotating coordinate system. In other cases more than one frequencies are present, which means that the solid body rotation is superimposed with a genuine oscillation of the flow pattern. When the ratio of the two periods are close to a small integer, “beating” can be observed in the monitored quantities. When many periods are present, the time variations become irregular, although the amplitude remains bounded. Table 1 summarizes the results and the observed periods for all cases.

Certain trends can be easily identified from the table. For a fixed shock distance  $r_{shock}$ , the larger the specific angular momentum  $\lambda$  is, the more and usually longer periods are observed. This can also be seen in Fig. 5, where the time variation of the total mass in a

angular sector  $0 < \varphi < 2\pi/3$  is plotted. The figure contains further information. Note that the higher  $\lambda$  is, the larger the average mass in the sector becomes, i.e. the further away the deformed shock is from the BH, since most of the mass is contained in the compressed post shock region. Furthermore, the amplitude of the mass variation also increases with  $\lambda$ , which corresponds to a larger radial extent of the asymmetric shock pattern. Even in the most unstable case 1d, however, the total mass in the sector increases by about 30% only.

A clean example of the “beating” phenomenon can be seen in Fig. 6, which shows the total mass variation in the same angular sector for case 2c. The Fourier spectrum of the time variation, obtained with a discrete FFT, shows two well defined peaks with almost identical amplitudes in Fig. 7. Since the ratio of the frequencies is close to 2, strong beating can be observed in the time variation.

The periods  $P$  are in the same range  $60 < P < 280$  for all cases listed in Table 1, despite the large variation in the rotation period at the shock distance, which is  $2\pi r_{shock}^2/\lambda$  and it varies roughly from 100 to 2000 for cases 1 to 5, respectively. The radial extent of the deformed shock is not too large in most cases, e.g. for cases 2a and 3 the radial shock distance varies between 9 to 11 and 13 to 16, respectively. In case 5b, however, the shock has reached the outer boundary, at  $r_{max} = 56$ , which is more than twice the shock distance  $r_{shock} = 23.4$  of the axially symmetric steady state.

## 5. Conclusions

We find that the axisymmetric shocks predicted by Chakrabarti’s theory (Chakrabarti 1990) in a rotating inviscid accretion flow are generally unstable to azimuthal perturbations, but *the instability saturates at a low level, and a new, stable, asymmetric configuration develops with a strongly deformed shock rotating steadily*. It is possible that shocks produced with very large angular momentum are unstable, in the sense that the perturbation triggers large deviations from the circular symmetry that extend up to the outer sonic point, but this does not happen in the test cases presented here.

The new disk is no longer axisymmetric despite that the boundary conditions are the same as initially: axially symmetric supersonic inflow at the outer and supersonic outflow at the inner boundary. According to the numerical simulations, the asymmetric shock configuration is continuously self sustained and self reproducing around the BH. In general, this asymmetric configuration of the flow speed, density, and temperature produces time variations in any measured quantities. For a fixed shock distance we find that the time variations are regular periodic for low angular momentum flows and they are more irregular,



containing more frequencies, for flows with a larger angular momentum.

The time variation could be observed and it could be a signature of the black hole’s presence. As it can be seen in Table 1, typical periods are in the range 60 to 300 in the dimensionless units. Taking  $P = 100$  as a typical case, we may convert it to physical units by multiplying with  $2GM/c^3 \approx 10^{-5}M/M_\odot$  sec. For a black hole of ten solar mass, this gives approximately 0.01 seconds, while a BH with  $M = 10^6M_\odot$  would produce oscillations typically with 1000 second periods.

We point out that although the general scenario seems different, there are similarities with the nonaxisymmetric disk instabilities studied by Blaes & Hawley (1988). Of course other important physical ingredients have to be included for a more realistic study of the shock behavior: full 3-dimensional treatment, physical viscosity, true cooling mechanism etc. Fully three dimensional simulations using the Versatile Advection Code of the same problem are in due course and will be presented in a forthcoming work. The role of the physical viscosity should also be further investigated, since in general, as shown in a similar context (cfr. Lanzafame, Molteni, & Chakrabarti 1998), but in axisymmetric conditions, moderate viscosity may produce changes in the shock structure and induce oscillations, while a large viscosity may stabilize the flow in a Keplerian regime, eliminating the shocked solutions. Our convergence studies indicate that the azimuthal instability is not very sensitive to a small amount of “numerical viscosity”. In any case we note that it has already been shown by time independent studies that the inner part of canonical accretion disks may have supersonic flows even for the viscosity parameter  $\alpha$  about 0.01 (Chakrabarti, 1996) or even larger (Igumenshev, Abramowicz, & Novikov 1998).

Our investigation is intended as a first exploration of the new axially asymmetric solutions. Despite the many simplifying assumptions, we suggest that such a phenomenon may occur easily in real physical systems when viscosity is small and initial angular momentum is sub-Keplerian since the parameter range that leads to shocked solutions is fairly large and the perturbation required to trigger the asymmetric configuration is very small. The azimuthal instability described in this paper, in any case, is a fine example of how non linearity of the fluid dynamic equations may break the symmetry of the initial and boundary conditions.

VAC was developed by G.T. as part of the project on ‘Parallel Computational Magneto-Fluid Dynamics’, funded by the Dutch Scientific Research Foundation (NWO) Priority Program on Massively Parallel Computing. The first simulations were done on a Cray C90 for which computer time was sponsored by the Dutch National Computing Facilities Foundation (NCF). G.T. currently receives a postdoctoral fellowship (D 25519)

from the Hungarian Science Foundation (OTKA). O.A.K. was supported by the Russian Foundation for Basic Research (grant 97-02-16486). Both G.T. and O.A.K. thank the University of Palermo for its hospitality during their visits.

### A. Algebraic Equations for 1D Steady State Solution

Here we give a method to calculate the 1D steady state solution, in particular the scaled accretion rate  $A/\rho(r_{max})$  and the shock position  $r_{shock}$  as a function of the specific angular momentum  $\lambda$  and the Bernoulli constant  $B$ . This method requires (iterative) solutions of algebraic equations without the need to integrate ordinary differential equations (cfr. Chakrabarti 1989, 1990 for a method using integration).

Let us introduce the sound speed  $a = (\gamma p/\rho)^{1/2}$  and the Mach number in the radial direction  $\mathcal{M} = -v_r/a$ . In case of an axially symmetric one dimensional steady state, i.e.  $\partial/\partial t = \partial/\partial \varphi = \partial/\partial z = 0$ , we can integrate (2), (4), and (5) to obtain three conserved quantities,  $A = r\rho v_r$ ,  $\lambda = rv_\varphi$ , and  $B = (e + p)/\rho + \Phi$ , respectively. For any continuous isentropic solution, the density and the sound speed are related as  $\rho = Ca^{2/(\gamma-1)}$ , where  $C$  is a constant for the particular solution. We may now proceed to eliminate  $\rho$ ,  $v_r$ ,  $v_\varphi$ ,  $p$ , and  $e$  in favor of the conserved quantities  $A$ ,  $B$ ,  $C$ , and  $\lambda$ , and the single unknown function, the Mach number  $\mathcal{M}(r)$ . First  $a^2$  should be expressed from the Bernoulli equation

$$B = \frac{1}{2}(\mathcal{M}a)^2 + \frac{\lambda^2}{2r^2} + \frac{a^2}{\gamma-1} - \frac{1}{2(r-1)} \quad (\text{A1})$$

then it can be substituted into the mass conservation equation

$$A = -r\rho v_r = Cr\mathcal{M}a^{\frac{\gamma+1}{\gamma-1}} \quad (\text{A2})$$

to arrive at the final equation for  $\mathcal{M}(r)$

$$\frac{A}{C} = f(\mathcal{M}) \cdot g_{\lambda,B}(r) \quad (\text{A3})$$

with

$$f(\mathcal{M}) = \frac{\mathcal{M}}{\left[\frac{1}{2}\mathcal{M}^2 + \frac{1}{(\gamma-1)}\right]^{\frac{\gamma+1}{2(\gamma-1)}}} \quad (\text{A4})$$

and

$$g_{\lambda,B}(r) = r \cdot \left[ B - \frac{\lambda^2}{2r^2} + \frac{1}{2(r-1)} \right]^{\frac{\gamma+1}{2(\gamma-1)}} \quad (\text{A5})$$

The  $f$  function has a single maximum at  $\mathcal{M} = 1$ , and it can be inverted both in the subsonic  $0 \leq \mathcal{M} < 1$  and supersonic  $\mathcal{M} > 1$  regions. The  $g$  function has in general two

local minima at  $r_1$  and  $r_2$  with  $r_1 > r_2$ , which can be determined by solving the algebraic equation  $dg/dr = 0$  numerically.

At large distances from the BH, the Mach number is  $\mathcal{M} \ll 1$ , while close to the horizon  $\mathcal{M} \gg 1$ , thus any continuous solution has to have a sonic point with  $\mathcal{M} = 1$ , where  $f[\mathcal{M}(r)]$  has a maximum. Since the  $f(\mathcal{M}) \cdot g(r)$  product must be constant along the flow (A3), the maximum of  $f$  should be at one of the minima of  $g$ , i.e. at  $r_1$  or  $r_2$ . Therefore we can have two isentropic solutions  $\mathcal{M}_1$  and  $\mathcal{M}_2$

$$\mathcal{M}_{1,2}(r) = f^{-1} \left[ \frac{f(1)g_{\lambda,B}(r_{1,2})}{g_{\lambda,B}(r)} \right] \quad (\text{A6})$$

where we use the subsonic branch of  $f^{-1}$  for  $r < r_{1,2}$  and the supersonic branch for  $r > r_{1,2}$ .

The outer boundary conditions can now be easily determined from the  $\mathcal{M}_1(r)$  solution, which connects the outer sonic point at  $r_1$  with the boundary located at  $r_{max}$ . First  $\mathcal{M}_1(r_{max})$  is calculated from the algebraic equation (A6), then the sound speed  $a(r_{max})$  from (A1), and finally the radial inflow speed  $v_r = -\mathcal{M}_1 a$  can be obtained. The scaled accretion rate is  $A/\rho(r_{max}) = -r_{max}v_r(r_{max})$ .

A standing shock can occur in the solution at  $r_{shock}$  if  $\mathcal{M}_1(r_{shock}) > 1$  and  $\mathcal{M}_2(r_{shock}) < 1$  are related by the Hugoniot relation

$$\mathcal{M}_2 = h(\mathcal{M}_1) \equiv \left[ \frac{2 + (\gamma - 1)\mathcal{M}_1^2}{2\gamma\mathcal{M}_1^2 - (\gamma - 1)} \right]^{1/2} \quad (\text{A7})$$

First  $\mathcal{M}_1(r_{shock})$  can be determined by solving the algebraic equation

$$\frac{f(\mathcal{M}_1)}{f[h(\mathcal{M}_1)]} = \frac{g_{\lambda,B}(r_1)}{g_{\lambda,B}(r_2)} \quad (\text{A8})$$

next the shock position  $r_{shock} = g_{\lambda,B}^{-1}[f(1)g_{\lambda,B}(r_1)/\mathcal{M}_1(r_{shock})]$  can be calculated. In general there can be two solutions, but only the outer one is stable (Nakayama 1994).

## REFERENCES

- Blaes, O. M., & Hawley, J. F. 1988, *ApJ*, 326, 277
- Chakravarthy, S., & Osher S. 1985, AIAA Paper No. 85-0363
- Chakrabarti, S. K. 1989, *ApJ*, 347, 365
- Chakrabarti, S. K. 1990, *Theory of Transonic Astrophysical Flows*, (Singapore: World Scientific)
- Chakrabarti, S. K., & Molteni, D. 1993, *ApJ*, 417, 671
- Chakrabarti, S. K., & Molteni, D. 1995, *MNRAS*, 272, 80
- Chakrabarti, S. K. 1996, *ApJ*, 464, 664
- Gammie, C. F. & Popham, R. 1998, *ApJ*, 498, 313
- Harten, A. 1983, *J. Comput. Phys.*, 49, 357
- Hawley, J. F., Smarr, L. L., & Wilson, J. R. 1984a, *ApJ*, 277, 296
- Hawley, J. F., Smarr, L. L., & Wilson, J. R. 1984b, *ApJS*, 55, 211
- Igumenshev, I. V., Abramowicz, M. A. & Novikov I. D. 1998, *MNRAS*, 298, 1069
- Kuznetsov, O. A., Lovelace, R. V. E., Romanova, M. M., & Chechetkin, V. M. 1998, *ApJ*, (submitted)
- Lanzafame, G., Molteni, D., & Chakrabarti, S. K. 1998, accepted by *MNRAS*.
- Lu, J., & Yuang, F. 1997, *PASJ*, 49, 525
- Molteni, D., Lanzafame, G., & Chakrabarti S. K. 1994, *ApJ*, 425, 161
- Nakayama, K. 1993, *PASJ*, 45, 167
- Nakayama, K. 1994, *MNRAS*, 270, 871
- Narayan, R., Mahadevan, R. & Quataert, E. 1998, *The Theory of Black Hole Accretion Discs*, eds. M.A. Abramowicz, G. Bjornsson & J.E. Pringle (Cambridge)
- Paczynski, B., & Wiita, P. J. 1980, *A&A*, 88, 23
- Roe, P. L. 1986, *Ann. Rev. Fluid Mech.*, 18, 337
- Ryu, D., Brown, G. L., Ostriker, J. P., & Loeb A. 1995, *ApJ*, 452, 364
- Tóth, G. 1996, *Astrophys. Lett. & Comm.*, 34, 245
- Tóth, G. 1997, in *High Performance Computing and Networking Europe 1997 Conf.*, ed. B. Hertzberger, & P. Sloot (Berlin: Springer-Verlag), *Lecture Notes in Computer Science*, 1225, 253

- Tóth, G., & Odstrčil, D. 1996, *J. Comput. Phys.*, 128, 82
- Tóth, G., Keppens, R., & Botchev, M. A. 1998, *A&A*, 332, 1159
- Yukawa H., Boffin H. M., Matsuda T., 1997, *MNRAS*, 292, 321
- Vyaznikov, K. V., Tishkin, V. F., & Favorsky, A. P. 1989, *Mathematical Modeling*, 1, 79  
(in Russian)

Fig. 1.— Shock location  $r_{shock}$  versus the Bernoulli constant  $B \equiv (e + p)/\rho + \Phi$  is plotted for different values of the specific angular momentum  $\lambda \equiv rv_\varphi$ .

Fig. 2.— Contourlines of density are shown at four different times  $t$ . The simulation is done in  $r, \varphi$  coordinates, but the picture is shown in the  $x, y$  plane for easier interpretation. The initial perturbation has not reached the circular shock in the upper left snapshot, and it just crosses the shock front at  $t = 24$ . The new twisted shock appears after a long time  $t \approx 1000$  and it remains stable indefinitely. The parameters of this simulation are similar to those of case 2a in Table 1.

Fig. 3.— Contour plot of the radial Mach number  $|v_r|/a$  for the last snapshot ( $t = 13459$ ) of Fig. 2. Contourlines in the subsonic region (Mach number below unity) are suppressed so that the shock location is shown as the last contour line of the incoming accretion flow. The inner region with unresolved contourlines corresponds to the supersonic region of the postshock infall. The Schwarzschild radius is indicated with the innermost dotted circle.

Fig. 4.— Wire frame representation of pressure  $p$  and radial Mach number  $v_r/a$  in the polar coordinates  $r, \varphi$ . The black hole is at  $r = 0$  just outside the right boundary. For sake of clarity only 50 grid lines are drawn in both directions, but the actual resolution is  $200 \times 100$ . The shock happens to close back into itself at  $\varphi \approx \pi$ . The density contourlines corresponding to this snapshot are shown in the left bottom panel of Fig. 2.

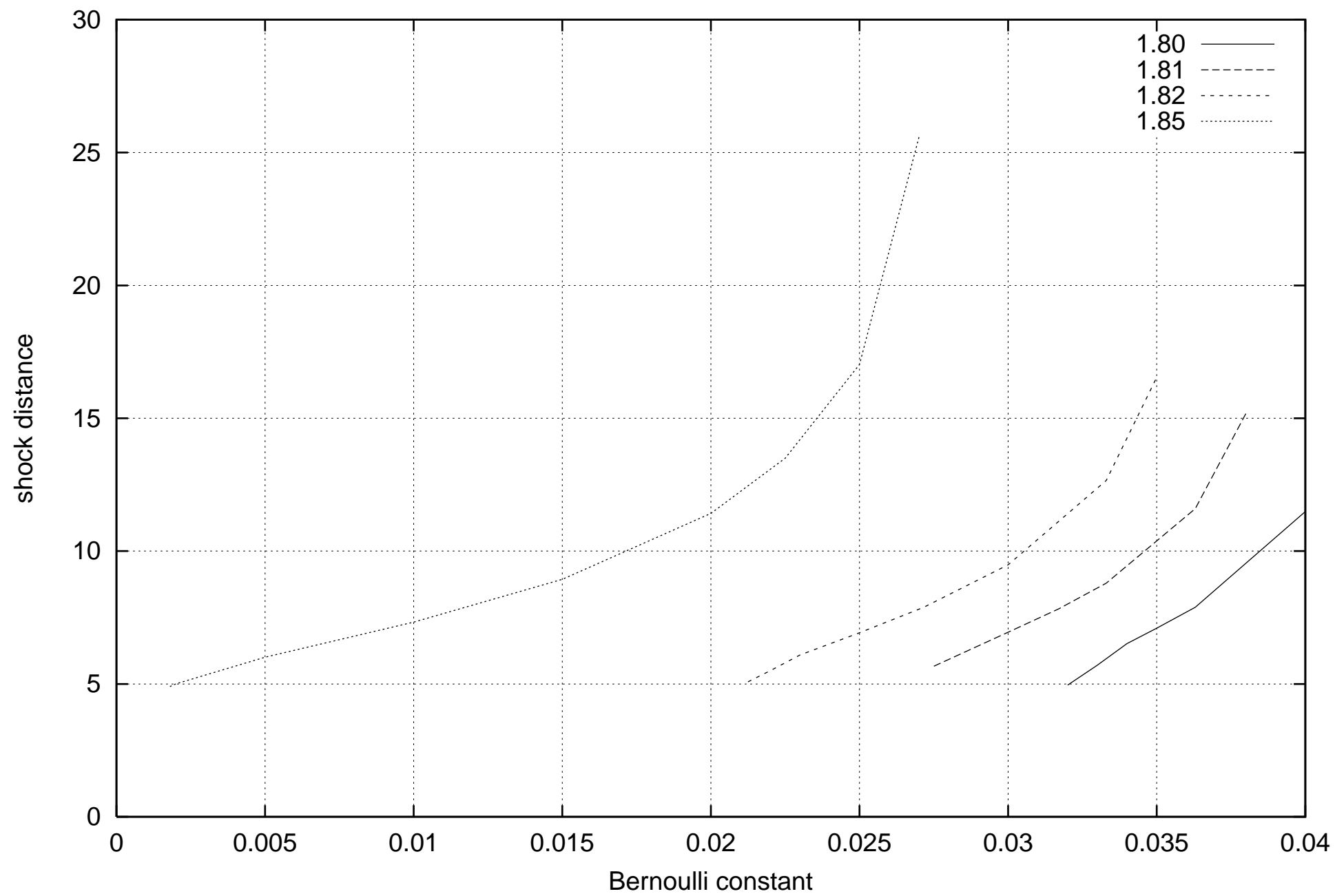
Fig. 5.— Time variation of the total mass in an angular sector  $0 < \varphi < 2\pi/3$  for cases 1a, 1b, and 1d, i.e. fixed shock distance  $r_{shock} = 5.3$  with increasing specific angular momentum  $\lambda$ . The cases were run until the amplitudes of the oscillations became bounded, thus the curve for case 1a is in the lower left part of the plot.

Fig. 6.— Time variation of the total mass in an angular sector  $0 < \varphi < 2\pi/3$ .

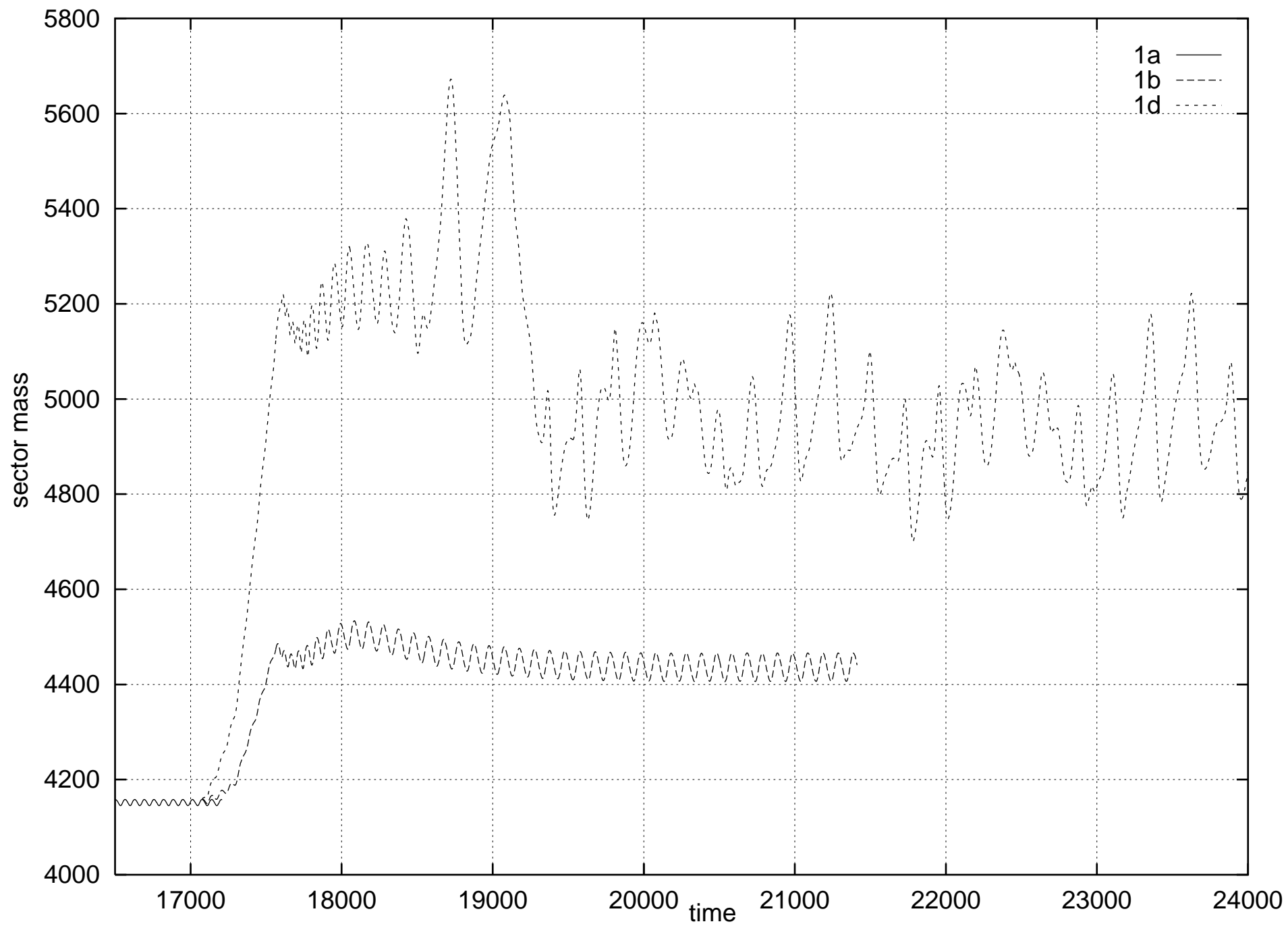
Fig. 7.— Fourier transform of the time variation shown in Fig. 6. Note the two distinct peaks in the Fourier spectrum at  $P = 134$  and  $P = 259$  with almost equal amplitudes. The closeness of the period ratio to 1:2 is responsible for the “beating”.

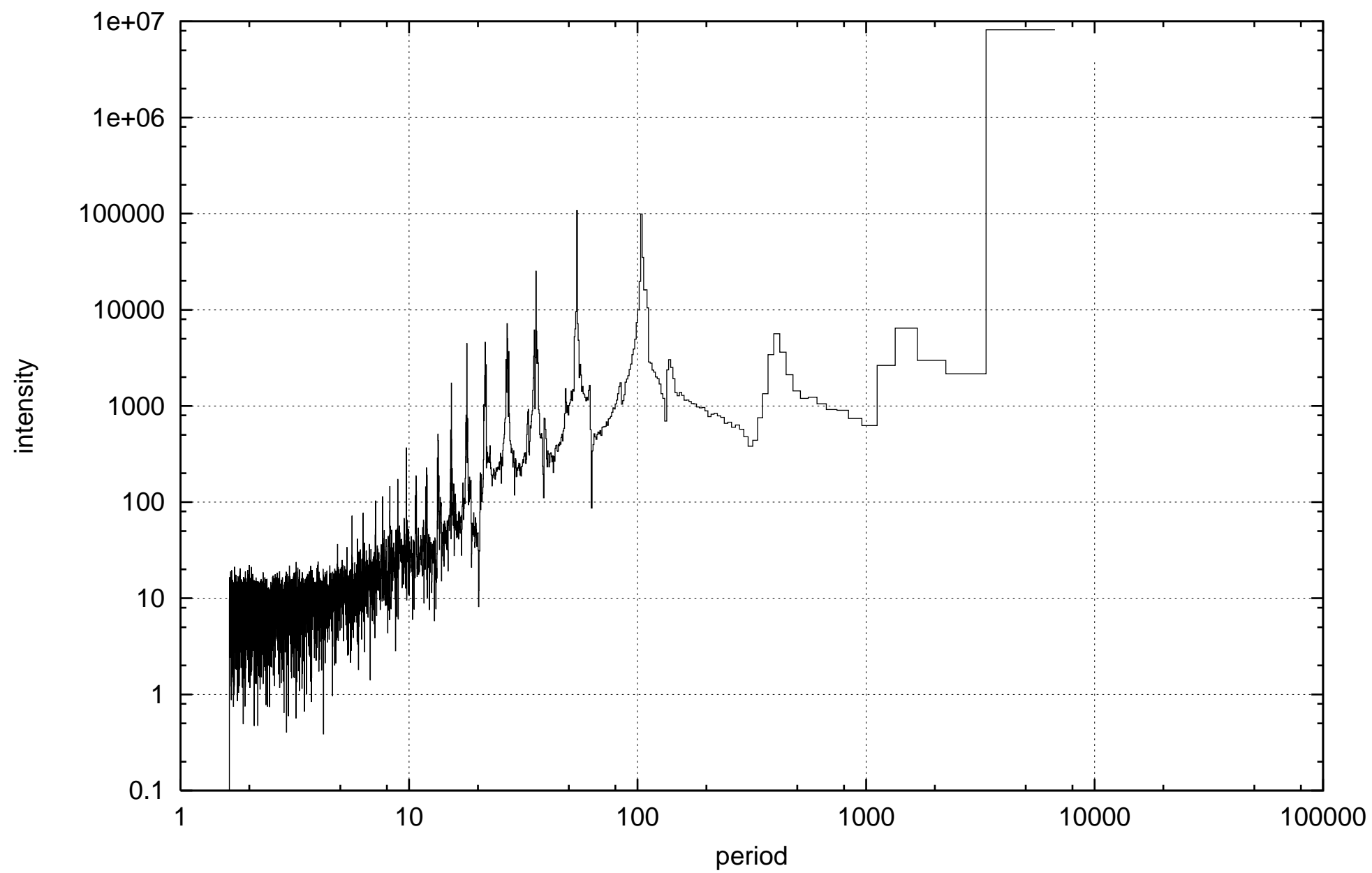
Table 1. Simulation Parameters and Results

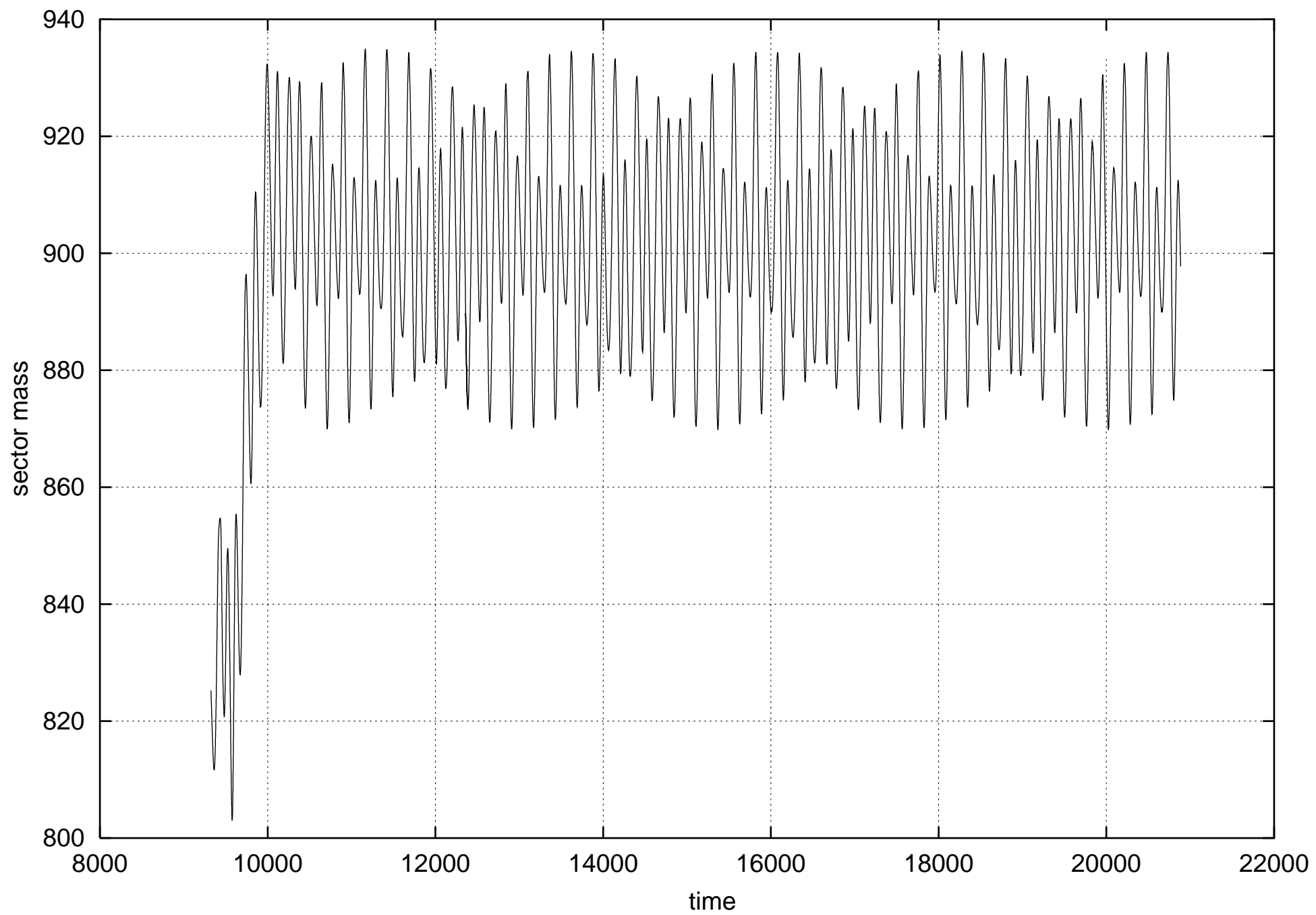
case	$r_{shock}$	$A/\rho(r_{max})$	$\lambda$	$B$	$P$	comment
1a	5.3	4.0890	1.7770	.04333	63	regular osc.
1b	5.3	4.4984	1.8000	.03220	98	regular osc.
1c	5.3	4.7262	1.8100	.02701	111,209	beating
1d	5.3	5.1041	1.8225	.02000	...	irregular
2a	7.8	3.0000	1.8000	.03630	125	regular osc.
2b	7.8	3.0896	1.8100	.03170	242,270	beating
2c	7.8	3.1834	1.8200	.02715	134,259	beating
3	12.7	3.3450	1.8200	.03332	215	regular osc.
4	17.2	4.2750	1.8255	.03331	...	nearly stable
5a	23.4	4.8766	1.8620	.02307	273	regular osc.
5b	23.4	5.0442	1.8720	.02000	...	leaves domain



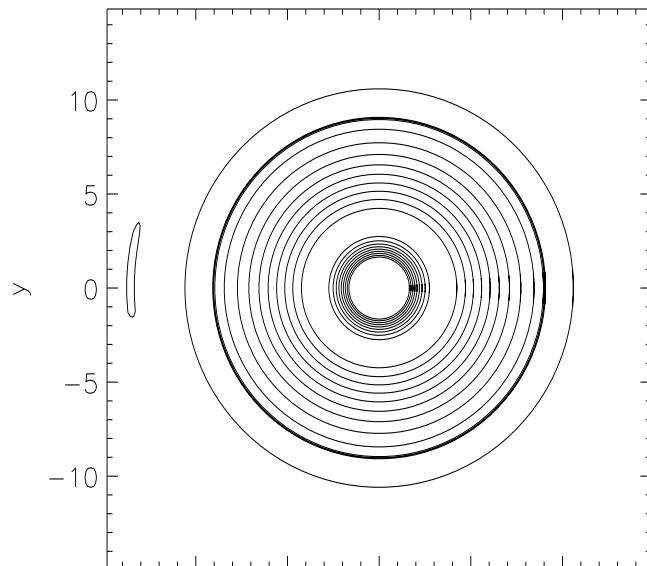




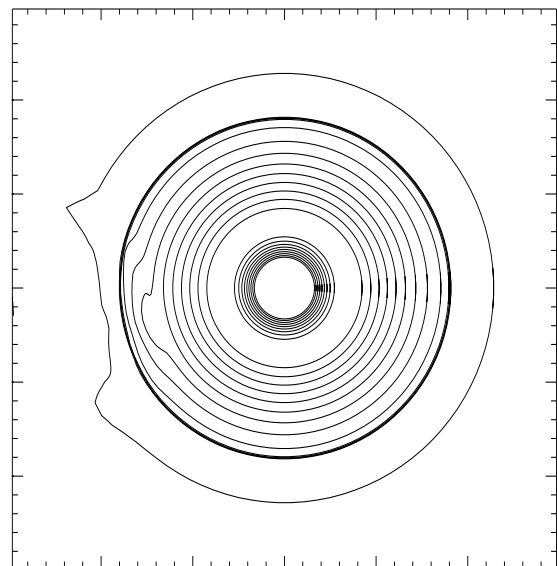




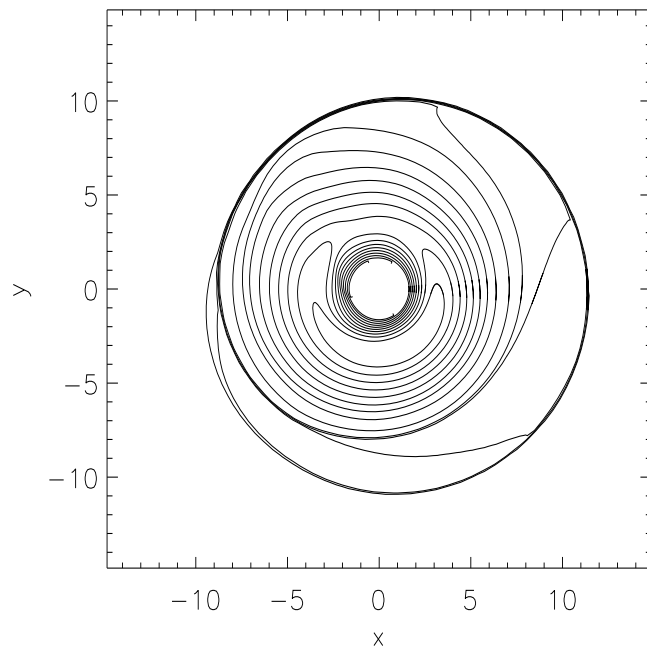
t=6



t=24



t=1542



t=13459

